Environmental Science & Technology

pubs.acs.org/est

Article

Sorption Behavior and Aerosol–Particulate Transitions of ^{7}Be, ^{10}Be, and ^{210}Pb: A Basis for Fallout Radionuclide Chronometry

Joshua D. Landis,* Carl E. Renshaw, and James M. Kaste

Cite This: *Environ. Sci. Technol.* 2021, 55, 14957–14967

Read Online

ACCESS | Metrics & More | Article Recommendations | Supporting Information

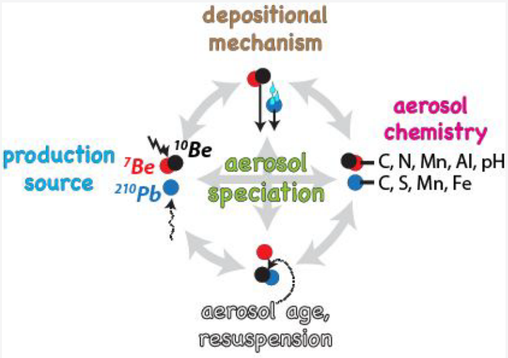

ABSTRACT: We investigated the partitioning of ^{7}Be, ^{10}Be, and ^{210}Pb aerosols between operationally dissolved and >0.5 μm particulate fractions in wet and dry atmospheric deposition. Bulk deposition *in situ*-log(K_D) averaged 4.27 ± 0.46 for ^{7}Be and 4.79 ± 0.59 for ^{210}Pb (±SD, $n = 163$), with corresponding activity-fractions particulate (f_P) = 24 and 48%. K_D was inversely correlated with particulate mass concentration (p_C), a particle concentration effect (p.c.e.) that indicates that dissolved ^{7}Be and ^{210}Pb are bound to submicron colloids. Experimental desorption-K_D was higher than *in situ* by a factor of 20 for ^{7}Be and 4 for ^{210}Pb ($n = 27$), indicating that FRN sorption to particulates was irreversible. ^{7}Be:^{10}Be ratios confirmed that colloidal and particulate fractions were geochemically distinct, with corresponding ages of 120 ± 30 and 260 ± 45 days, respectively [mean ± SE, $n = 9$, $p = 0.011$]. Fractions particulate f^{Be7}, f^{Be10}, and f^{Pb210} each increased with ^{7}Be:^{10}Be bulk age, a particle-age effect (p.a.e). In multiple regression, f^{Be7} was best predicted by N, Mn, Al, and Ni [$R^2 = 0.75$, $p < 0.0001$], whereas f^{Pb} relied on N, S, Fe, and Mn [$R^2 = 0.69$, $p < 0.0001$]. Despite differences in magnitude and controls on partitioning, the ratio f^{Be}:f^{Pb} converged to 1 with p_C in the range of 10–100 mg L^{-1}. Given sufficient solid surfaces, irreversible sorption and p.a.e. form a basis for ^{7}Be:^{210}Pb chronometry of aerosol biogeochemical cycling.

KEYWORDS: *FRN, aerosol, ^{7}Be, ^{10}Be, ^{210}Pb, sorption, partitioning, speciation, atmosphere, deposition, distribution*

■ INTRODUCTION

Atmospheric aerosols play critical roles in Earth systems, from climate forcing[1−3] to biogeochemical cycles[4,5] to toxicology of fine particulate matter (PM2.5) and associated metals including Hg, Pb, Cu, Fe, Mn, Ni, V, and Zn.[6−9] Progress in each of these venues is limited by uncertainties in how aerosols interact with the biogeosphere through rates of scavenging and resuspension.[1,10−13] The natural fallout radionuclides (FRNs) ^{7}Be, ^{10}Be, and ^{210}Pb might provide new insights into aerosol dynamics because they have well-defined atmospheric sources and are distributed universally. Moreover, the radioactive decay of FRNs poses the opportunity to develop chronologies of aerosol processes, linking the fates of atmospherically deposited elements with time scales of their deposition and terrestrial redistribution.[14,15] However, the transition from atmosphere to biogeosphere remains an open frontier in FRN systematics: what do the FRNs truly trace?

The FRNs are produced in the atmosphere, both ^{7}Be (half-life 54 days) and ^{10}Be (half-life 1.4 × 10^{6} years) by cosmogenic spallation of N_2 and O_2, and ^{210}Pb (half-life 22.3 years) by radiogenic decay of gaseous ^{222}Rn which emanates from ubiquitous ^{238}U-bearing soils and sediment. Following production, each FRN sorbs irreversibly to ambient aerosols to trace atmospheric circulation[16−19] and upon wet and dry deposition from the atmosphere follows pedogenic and geomorphic processes.[15,20−29] Typically, these applications rely on a key assumption that, with high partition coefficients (K_D) on the order of 10^{4}–10^{5}, the FRNs are particle-reactive and trace bulk aerosol, soil, and sediment. Speciation of the FRNs within these settings is not known, however, and limitations of current applications are uncertain. The characteristics of ^{7}Be, ^{10}Be, and ^{210}Pb in relation to each other are especially important since the FRNs can be combined as chronometers, provided that their behaviors are shown to be congruent.[30,14,15]

Specific minerals, ligands, or macromolecules that FRNs may favor in sorption are becoming a focus of experimental work.[31−35] Contextualizing experimental results remains a challenge, however, due to the complexity and breadth of geochemical systems. FRN speciation is determined by interacting cofactors including production source, depositional process, aerosol chemistry, and particle age, and through these factors, FRN atmospheric deposition represents multiple

Received: May 16, 2021
Revised: September 23, 2021
Accepted: September 24, 2021
Published: October 8, 2021

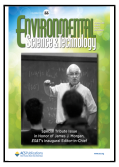

aerosol populations.[36] Further, upon interaction with terrestrial particulate matter (PM), the speciation of FRNs is likely to evolve with different mixtures of primary minerals, surface coatings, and organic compounds.[37−39] Faced with this complexity, a central challenge to FRN applications remains: do the beryllium isotopes ^{7,10}Be and ^{210}Pb trace congruent pathways via bulk aerosol, soil, and sediment, or are they fractionated through associations with specific aerosol and particulate populations?

Here, we approach the complexity of FRN speciation using the "natural experiment" of atmospheric deposition. We assess the partitioning of FRNs to ambient PM in 3 years of continuous, weekly measurements (n = 163), separating 0.5 μm filter-passing and filter-retained fractions in bulk deposition. To probe environmental factors that control FRN partitioning, we use multivariate statistics and a large number of measurements representing all seasons and a range of meteorological conditions, variations in pH, and concentrations of major/trace elements (MTEs), particulate mass (p_C), carbon (C_C), and nitrogen (N_C). Among MTEs, we describe both operationally dissolved (<0.5 μm) and weak-acid-soluble (2% HCl) fractions, interpreting the latter as environmentally relevant and indicative of insoluble aerosols, particles, and surfaces that regulate FRN partitioning.[40−43] Following a discussion focused on ^{7}Be and ^{210}Pb, we introduce ^{10}Be measurements for a small subset of samples to aid interpretation of differences between ^{7}Be and ^{210}Pb. Unlike ^{7}Be and ^{210}Pb, isotopes of Be should not fractionate, and variations in ^{7}Be:^{10}Be ratios can thus be attributed to mean aerosol age.[44]

■ EXPERIMENTAL SECTION

Sample Collection. This study was performed on the Dartmouth College campus in the College Park, a 7 hectare urban mixed forest of oak (*Quercus* sp.), maple (*Acer* sp.), spruce (*Picea* sp.), and pine (*Pinus* sp.). Between September 2017 and September 2020, we collected 163 weekly samples of bulk atmospheric deposition in tandem "A" and "B" polyethylene collectors (volume = 20 L, area = 650 cm^2, surface area index = 5.2) placed at a height of 40 cm above grassy lawn. The "A" collections represent a subset of an ongoing 9 year study of bulk deposition (n = 461) described elsewhere.[36] Analytical methods are illustrated in Figure SI 1.

Ambient aerosols with a mean aerodynamic diameter of <10 μm (PM10) were collected on quartz filters (Mesa Laboratories, 47 mm) in time intervals coincident with bulk deposition using a BGI PQ200 automated sampler (Mesa Laboratories, Lakewood CO) operated continuously at 16.7 L min^{-1} (n = 128).

Seasons were defined and abbreviated as follows: winter (0) = Dec.−Feb., spring (1) = Mar.−May, summer (2) = June−Aug., autumn (3) = Sep.−Nov.

Nonacidified "B" Collector. We deployed a nonacidified ("B") collector to assess FRN partitioning between filter-passing and filter-retained fractions, which we separated using binderless, high-purity 0.5 μm quartz-fiber filters (Advantec QR-100, 47 mm diameter). The "B" collector should be viewed as a batch reactor because it aggregates FRNs, aerosols, and particulate matter from multiple ambient sources. The aggregate mixture is determined by the "natural experiment". We estimated an effective reaction time within the collector as the FRN flux-weighted elapsed time between precipitation events and sample collection.

Acidified "A" Collector. The second "A" collector was acidified (2% HCl) to assess FRN mass balance in the "B" collector, since trace metals may be lost to collector surfaces when not acidified.[45,31] By comparing "A and "B" collector totals, we determined that flux-weighted losses from the "B" averaged 14.2 ± 1.4% for ^{7}Be and 18.0 ± 2.0% for ^{210}Pb (±SE, n = 139(14)). We omitted these fractions from partitioning calculations, since they cannot be unambiguously attributed to either filtered fraction.[31] Our comparison of A/B collectors is described in the Supporting Information and Figure SI 2.

Openfall−Throughfall (OF−TF) Collectors. We complemented weekly bulk collections with paired event-based, wet-only collections of openfall (OF; n = 30) and throughfall (TF; n = 53). TF samples were collected under the midpoint of mature canopies of red oak (*Quercus rubra*), Eastern white pine (*Pinus stroba*), and Norway spruce (*Picea abies*) and processed following "B" protocols.

FRN Measurements and Partitioning Metrics. ^{7}Be and ^{210}Pb in bulk deposition and PM10 were measured directly on 47 mm filters using gamma spectrometry. Instrumental analysis is described by Landis et al.[46] External calibration uncertainties were verified with the U/Th ore DL-1a (Canadian Certified Reference Material Project, Ottawa), mounted on 47 mm filters in small 50 mg aliquots to prevent self-absorption effects. Calculated DL-1a activities were within 2% of certified values for all U-series radionuclides across all detectors. Filter-retained "B" fractions were measured as collected on 47 mm filters. Total "A" and filter-passing "B" fractions were measured following preconcentration by MnO$_2$ coprecipitation (Supporting Information). Propagated analytical uncertainties were typically ca. 4% relative standard deviation (RSD) for ^{7}Be and 10% for ^{210}Pb.

Partitioning of FRNs was quantified as the equilibrium distribution coefficient, K_D

$$K_D = \frac{A^{>0.5}/M}{A^{<0.5}/V} = \frac{A^{>0.5}}{A^{<0.5}\cdot p_C} \tag{1}$$

where A = measured activity [Bq], M = >0.5 μm particulate mass, V = precipitation volume, and p_C = total particle mass concentration [mg L^{-1}].

We also defined the activity fraction particulate, f_P, as follows

$$f^{Be} \text{ or } f^{Pb}\,(\%) = \frac{A^{>0.5}}{A^{>0.5} + A^{<0.5}} \times 100 \tag{2}$$

We note that f_P is explicitly related to the product $K_D{\cdot}p_C$ as follows

$$f_P = 1 - \frac{1}{1 + K_D{\cdot}p_C} \tag{3}$$

Environmental Variables. Major and trace elements (MTEs) were measured by axial-view ICPOES (Spectro ARCOS). Details are provided in the Supporting Information. An operationally dissolved fraction of MTEs (abbreviated *d*.Al, etc.) was measured with 20 mL aliquots from the "B" collector, first filtered through 0.45 μm Nylon syringe filters and then acidified (2% HCl). An operationally soluble fraction of MTEs (abbreviated *s*.Al, etc.) was measured from aliquots taken from the "A" collector where acidification (2% HCl) preceded filtration with 0.5 μm quartz filters. Comparison of *d*. and *s*.

concentrations provided an index ($k.$) of relative MTE solubility[40,36]

$$k.\ \text{Al, etc.} = (A/B - 1) \times 100\% \tag{4}$$

The pH of "B" collections was measured using both epoxy and ROSS-type electrodes, calibrated daily with low-ionic-strength buffers (Fisher Scientific). Agreement between the electrodes was good with a mean difference = 0.02 ± 0.11 pH units (±SD, $n = 97$).

Total masses of C and N in the >0.5 μm particulate fraction (TC and TN) were measured using a Shimadzu TOC combustion analyzer on 6 mm punches subsampled from quartz filters. Particulate carbon (C_C) and nitrogen concentrations (N_C) were calculated as TC or TN divided by precipitation volume (V). TC by combustion includes both organic carbon (ca. 50% aerosol mass) and elemental/black carbon (ca. 20% aerosol mass).

Meteorological influences on FRN deposition were summarized by categorization of three distinct storm types based on characteristic aerosol compositions.[36] Enriched or *E*-type storms (21% of total) were high-midlatitude cyclones (MLCs) or convective storms with cold fronts and continental storm tracks and were strongly enriched in ^{210}Pb, ^{7}Be, S, Fe, Al, Mg, Mn, V, and Hg. Depleted or *D*-type storms (12% of total) were low MLCs with marine storm tracks and warm fronts and were depleted in ^{210}Pb and both lithogenic and anthropogenic aerosols but not in ^{7}Be or biogenic elements N, P, K and C. Remaining normal or *N*-type storms (67% of total) were dominated by frontal precipitation and were otherwise considered typical.

Desorption Experiments. A subset of >0.5 μm "B" samples ($n = 30$) and tree leaves (*Quercus rubra*, $n = 4$) was leached in 1 L solutions of 2 mM $MgSO_4$ (pH 4.5 with HCl) to measure desorption of FRNs. "B" leachates were filtered back to their original filters and reanalyzed by gamma spectrometry; a desorbed fraction was calculated by the difference between measurements before and after leaching. Mean particle concentrations *in situ* and in desorption experiments were comparable (22 ± 71 versus 21 ± 34 mg L^{-1}, respectively). Leaf leachates were filtered at 0.5 μm, and filtrates were measured for FRNs following evaporation, aqua regia digestion, and MnO_2 coprecipitation.

^{10}Be Preparation and Measurements. A subset of paired "A" and "B" samples ($n = 18$) was processed for ^{10}Be measurements in the Dartmouth Cosmogenic Isotope Lab. Extraction and purification details are given in the Supporting Information. ^{10}Be was measured by accelerator mass spectrometry (AMS) at Lawrence Livermore National Lab. Sample ^{10}Be:^{9}Be ratios were in the 10^{-12}–10^{-13} range with typical analytical uncertainties of 3%. Procedural blank ratios were 10^{-15} to 10^{-17} and corresponded to 1.3×10^5 atoms of ^{10}Be for samples processed with our high-level spike and 1.4×10^4 for low-level ^{9}Be spikes.

Statistical Analyses and Multiple Regression. Statistical analyses were performed in JMP Pro 14.0.0. All parameters were transformed to give normal distributions. We used a series of statistical models to interrogate the FRN/MTE data set (Figure SI3), with emphasis on stepwise multiple regression (analysis of covariance, ANCOVA) to quantify independent effects for each of the multiple explanatory variables on a response variable when all other explanators are held constant.

We first constructed models with master environmental variables including pH, p_C, reaction time, season, ambient mean temperature, and meteorological storm type. Hereafter, these are called general models. To the general models, we next added stepwise, specific MTE explanators including total fluxes ($t.$), dissolved ($d.$) and soluble concentrations ($s.$), and relative solubilities ($k.$). Hereafter, these are called specific models. In stepwise regression, stronger explanators supersede and replace weaker ones in the final model.

For final models, we quantified the individual effect (e^*) of each independent, significant explanator on the variance of the response variable as follows

$$e^* = \frac{SS_i}{\sum_i^n SS} \cdot R^2 \tag{5}$$

where SS_i is sum-of-squares for each i variable, and R^2 is the total model coefficient of determination. Due to high colinearity among bulk deposition parameters, we computed variance inflation factors (VIFs) for each explanatory variable in a multiple regression. VIF calculates the underestimation of model coefficient standard errors that result from colinearity. VIFs were computed by rerunning regressions with each explanator rotated, in turn, as the model response variable. The VIF for each i variable was then calculated as $VIF_i = 1/(1 - R_i^2)$, where R_i^2 is the new model coefficient of determination. Standard error in model coefficients for each explanator i is inflated by factor = $(VIF_i)^{-1/2}$, and $VIF > 5$ was considered unacceptable.

Next, we estimated the magnitude of explanator effects on the response variable. For continuous variables, log–log model coefficients represent the fractional change in the response variable for a given change in explanatory variable. We report this magnitude (m^*) as the percent change in a response variable given a 100% increase (doubling) of the explanator, where β is the model coefficient

$$m^* = (2^{\beta} - 1) \times 100\% \tag{6}$$

For categorical explanators, we cite the difference in least-squares adjusted means (μ_i) between categories of maximum and minimum values

$$m^* = (10^{\mu_{max} - \mu_{min}} - 1) \times 100\% \tag{7}$$

RESULTS AND DISCUSSION

Aerosol Chemistry. Measurements of environmental variables, FRNs, and MTEs are summarized in Table SI 1 and Table SI 2. We used multiple regression to summarize the FRN/MTE chemistry of bulk deposition by identifying five classes of aerosol relevant to their deposition and speciation[36] (Figure SI 4): secondary aerosols (^{7}Be, ^{210}Pb, S); biogenic aerosols (N, C, K, P, Mn); anthropogenic aerosols (Cd, Co, Cr, Na, Ni, Pb, V, Zn); soluble mineral aerosol (Mg, Ba, Ca, Sr); and insoluble mineral aerosol (Al, Fe).

Partitioning Metrics *in Situ* and in Desorption. We used the partition coefficient K_D (eq 1) to evaluate FRN sorption behavior under three conditions of varying particulate types and concentrations (p_C). These were weekly bulk (wet-plus-dry) deposition ($p_C = 20$ mg L^{-1}), event-based (wet-only) deposition under open sky (openfall, OF; mean $p_C = 4$ mg L^{-1}) and under a forest canopy (throughfall, TF; mean $p_C = 19$ mg L^{-1}). Under all conditions K_D for ^{7}Be was significantly lower than for ^{210}Pb [$p < 0.0001$]. For bulk deposition,

$\log(K_D)$ for ^{7}Be averaged 4.26 ± 0.47 (mean ± SD, $n = 161$) and for ^{210}Pb averaged 4.79 ± 0.67. Bulk $\log(K_D)$ for ^{7}Be and ^{210}Pb was strongly correlated across all seasons [$R^2 = 0.42$, $p < 0.0001$].

The $\log(K_D)$ in bulk deposition was indistinguishable from wet-only OF for ^{7}Be but was significantly higher for ^{210}Pb [$p = 0.002$] (Figure 1). Bulk deposition was characterized by a higher p_C due to resuspended PM deposited during dry periods interceding storm events. Resuspended ^{210}Pb constitutes up to 5% of its annual flux[36] and could bias bulk deposition to a higher K_D if irreversibly bound to PM. For TF deposition, K_D values of both ^{7}Be and ^{210}Pb were significantly lower than bulk deposition (Figure 1). This is attributable to complexation of the FRNs by colloidal organic carbon produced in the tree canopy.[47,48]

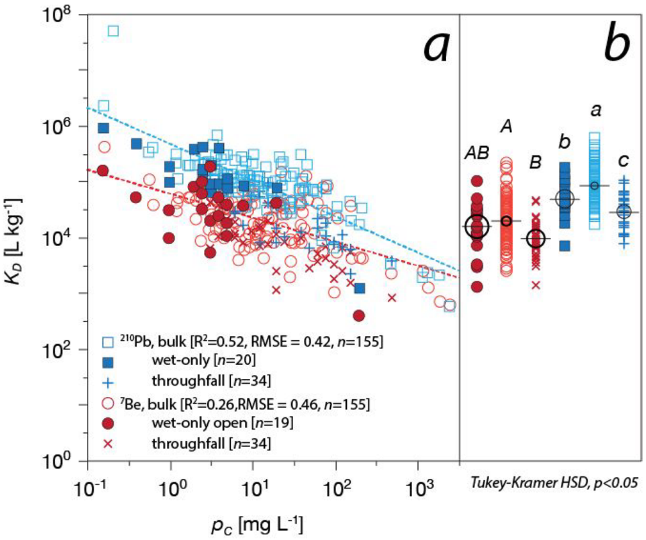

Figure 1. (a) Partition coefficients (K_D) for ^{7}Be and ^{210}Pb in atmospheric deposition as a function of particle mass concentration (p_C). Lines show linear fits to bulk deposition. (b) Residuals from linear fits to K_D vs p_C.

Bivariate correlations of K_D with environmental variables are given in Table SI 3. There was no pH dependence for either ^{7}Be or ^{210}Pb. Instead, the strongest control on K_D was an inverse correlation with p_C (Figure 1). This is a particle concentration effect (p.c.e.) widely observed in trace metal aqueous chemistry, indicating that FRN sorption to particulates does not conform to chemical equilibrium. The p.c.e. in experimental systems is attributed to irreversible sorption[49] or to nonlinear sorption isotherms.[50] In natural systems, the p.c.e. is attributed to submicron colloids that control the solubility of metals.[51−53] Especially for FRNs, the p.c.e. was not unexpected, since the typical diameter of both ^{7}Be and ^{210}Pb suspended aerosols is approximately that of the filter cutoff, about 0.5 μm.[54]

Nonequilibrium behavior has important implications for how FRNs might trace natural PM, since it implies that FRN sorption may be both preferential and irreversible. To assess the reversibility of FRN sorption, we performed a series of desorption experiments using bulk >0.5 μm particulate filters ($n = 30$) and tree leaves ($n = 4$). Pairwise, particulate desorption-K_D values were higher than those measured *in situ* for ^{7}Be by a factor of 23 [5.18 ± 0.59, mean ± SD, $n = 30$; $p < 0.0001$] and for ^{210}Pb by a factor of 5 [5.53 ± 0.13, $p < 0.0001$] (Figure 2). For perspective, the fraction of ^{7}Be activity

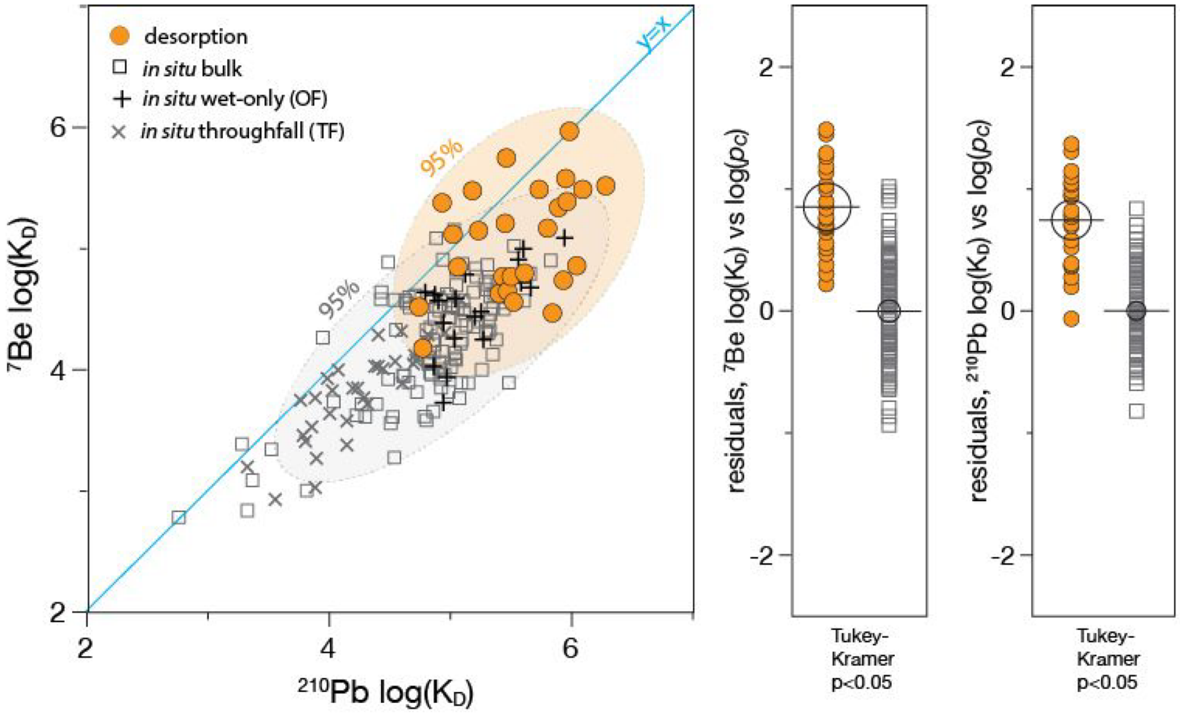

Figure 2. (a) Partition coefficients (K_D) for ^{7}Be and ^{210}Pb, compared for *in situ* bulk deposition and desorption experiments. *In situ* includes bulk deposition as well as wet-only openfall (OF) and throughfall (TF). For bulk deposition, mean pH = 4.9 and particulate concentration (p_C) = 14.9 mg L^{-1}; OF mean pH = 4.9, p_C = 3 mg L^{-1}; TF mean pH = 5.1, p_C = 23 mg L^{-1}. Desorption experiments were conducted with 2 mM $MgSO_4$ (pH = 4.5) with p_C = 18 mg L^{-1}. (b,c) Residuals from linear fits of K_D vs p_C analyzed by ANOVA against sample type.

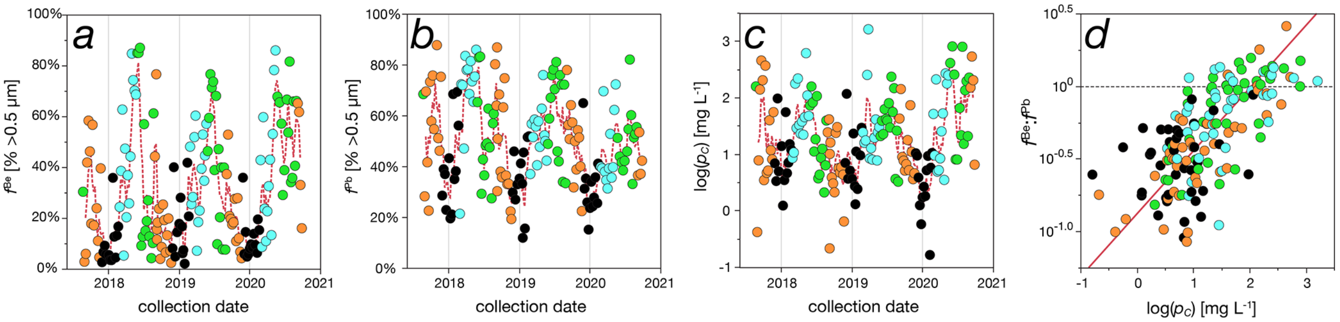

Figure 3. (a−c) Time-series for fractions particulate of ^{7}Be (f^{Be}) and ^{210}Pb (f^{Pb}) and particulate mass concentration (p_C) in bulk deposition. A 4 week running average is showing in dashed lines. (d) The ratio f^{Be}:f^{Pb} vs p_C. Symbols are color-coded by season for winter (black), spring (blue), summer (green), and autumn (orange).

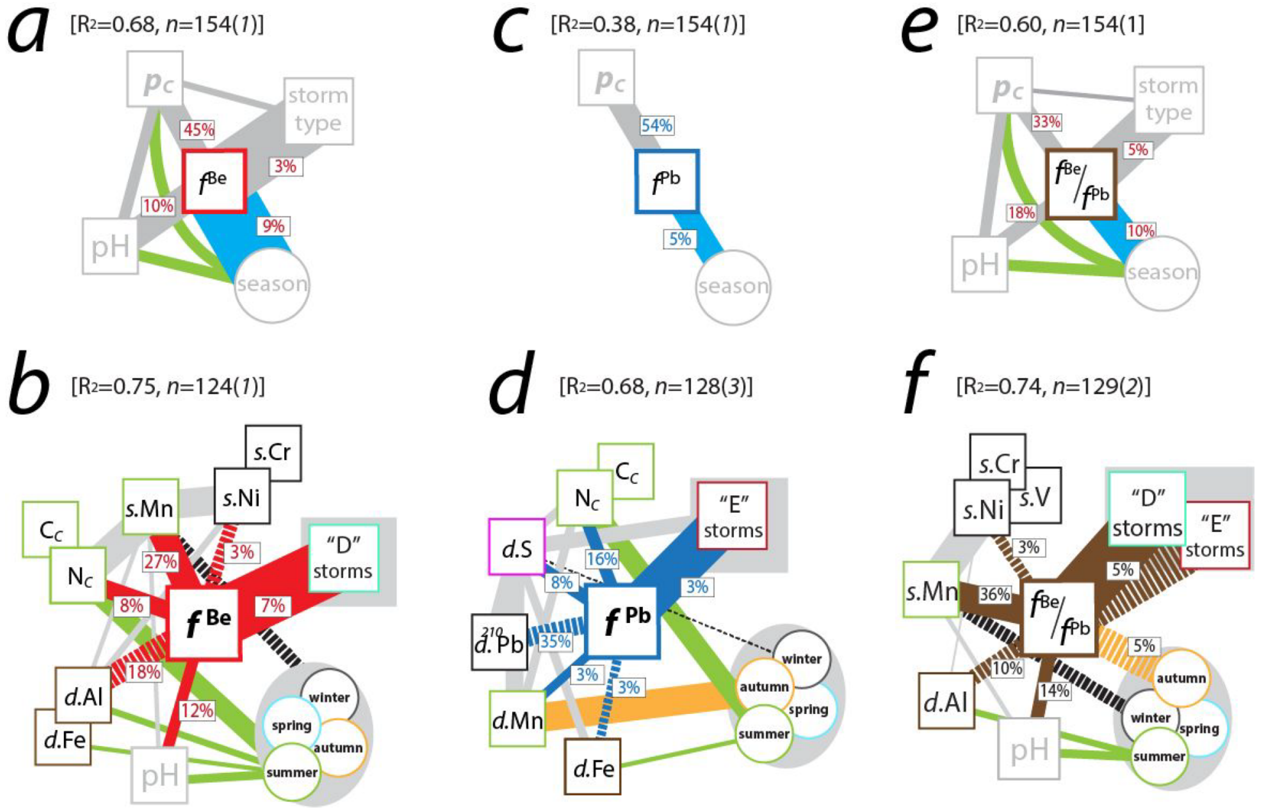

Figure 4. Multiple regression correlation webs for ^{7}Be and ^{210}Pb fractions particulate (f_P) and the ratio f^{Be}:f^{Pb}. General models using environmental factors pH, p_C, season, reaction time, and storm type are shown in (a,c,e). Specific models add major/trace element parameters (b,d,f). Lines connecting a central response variable with surrounding explanators indicate significant independent correlations [$p < 0.05$]. Dashed lines indicate inverse correlations. Line thicknesses are proportional to the magnitude of the explanator effect [m^*], and percentages indicate the fraction of total variance explained [e^*]. Overlapping variables show comparable but non-independent effects. Abbreviations: p_C (particle mass concentration), storm type *E* (continental) and *D* (marine), *s.* (soluble MTE fraction), *d.* (dissolved MTE fraction), N_C and C_C (particulate nitrogen and carbon concentrations).

desorbed was greater than for ^{210}Pb [p = 0.013], 28 ± 14 versus 12 ± 10%, respectively (mean ± SD). We cannot distinguish whether the desorbed FRN is truly dissolved or follows the release of colloidal material, but a much higher desorption K_D than *in situ* suggests that sorption is controlled by colloids rather than equilibrium desorption of dissolved species. In contrast to particulate filters, the fractions desorbed from tree leaves were indistinguishable for ^{7}Be and ^{210}Pb (7.5 ± 3.8, 7.3 ± 3.2%, respectively).

While the K_D values for both ^{7}Be and ^{210}Pb in atmospheric deposition are characteristically high, K_D can be misleading since a large fraction of FRNs remains operationally dissolved at low p_C.[55,56] Small differences or changes in K_D can thus translate into large environmental effects. As an alternative to K_D, we define f_P as the activity-fraction particulate according to eq 2. For ^{7}Be, $f_P{}^{Be}$ is log-normally distributed with a median = 19.8%, whereas $f_P{}^{Pb}$ is normally distributed with mean = 52.5% (Figure 3). Surprisingly, f_P shows no bivariate dependence on K_D for either ^{7}Be [p = 0.39] or ^{210}Pb [p = 0.31] (Table SI 4) but instead strong, positive correlations with p_C [R^2 = 0.58, $p <$ 0.0001; and R^2 = 0.40, p < 0.0001, respectively]. Consequently, both f_{Be} and f_{Pb} follow the seasonal pattern in p_C with the highest values in spring and summer and lowest in winter (Figure 3c). They are strongly (nonlinearly) correlated across seasons [R^2 = 0.47, p < 0.0001]. pH exerts a significant bivariate effect on $f_P{}^{Be}$ [R^2 = 0.28, p < 0.0001] and a minor, significant effect on $f_P{}^{Pb}$ [R^2 = 0.04, p = 0.018] (Table SI 4). In the range of p_C = 10−100 mg L^{-1}, the ratio f^{Be}:f^{Pb} converges to unity (Figure 3d).

Multiple Regression for ^{7}Be Partitioning. To quantify the simultaneous, independent effects of variables on FRN partitioning, we used analysis of covariance (ANCOVA). We first constructed a general model using environmental variables including pH, p_C, reaction time, season, ambient temperature, and meteorological storm type (see Methods and the Supporting Information). The general model explains $f_P{}^{Be}$ well using four explanators [R^2 = 68%; Figure 4a]. Here, p_C is predominant with a net effect [$e*$] explaining 41% of total variance in f^{Be}. pH is secondary [10%], followed by a seasonal effect with a spring/summer maximum and winter minimum [9%]. A meteorological effect [3%] biases $f_P{}^{Be}$ higher in marine moisture sources.[36]

Next, by adding specific MTE variables stepwise to the general model, we explain an additional 7% of variance in f^{Be} with a total of five explanators [R^2 = 0.75; Figure 4b]. The predominance of p_C is superseded by positive correlations with s.Mn [$e*$ = 27%] and total particulate nitrogen concentration, N$_C$ [8%] (and a similar, but not independent, effect from C$_C$). There are additional, inverse effects on f^{Be} from d.Al or d.Fe [18%] and d.Ni [3%]. The influence of pH remains [13%]. Seasonality is expressed only indirectly through the summer maximum of precipitation pH and spring/summer maximum of N$_C$ (Table SI 1). The meteorological bias of a marine source remains [6%], a source effect that is not explained with available MTE data. The modeled K_D for ^{7}Be has explanators and effects similar to those for f_P (s.Mn, s.V, d.Fe, N$_C$, pH), and these results are illustrated in Figure SI 5a.

In sum, ^{7}Be partitioning to the particulate fraction is strongly favored by N$_C$ and C$_C$, likely sourced from biogenic aerosols and organic matter. This is consistent with the formation of strong, inner-sphere complexes between ^{7}Be and organic ligands.[34] At the same time, dependence of f^{Be} on s.Mn is consistent with the importance of oxide surface coatings in driving ^{7}Be partitioning.[43] A significant pH effect describes the importance of Be aqueous chemistry, where the transition from BeOH$^+$ to Be^{2+} below pH ≈ 5 is widely implicated in its environmental behavior.[57,58] We also observe that increasing d.Fe, d.Al, s.Ni, and s.Cr each predict lower ^{7}Be partitioning, suggesting that ^{7}Be is regulated by Al and Fe colloidal phases and that it shares this behavior with other trace metals. In soil systems, Be mobility is linked to that of Al.[58,28] In aerosols, the solubility of both Al and Fe is maintained by organic ligands,[59,60] and Fe may be linked to redox recycling with other metals.[61] Collectively, our results suggest that the environmental fate of ^{7}Be hinges on interactions between organic matter and inorganic surfaces that promote binding,[37] and that this behavior is likely to be shared with Fe, Al, and certain anthropogenic metals. That N$_C$ and marine storms appear in models of both ^{7}Be speciation and atmospheric flux[36] is an important observation suggesting that ^{7,10}Be speciation established during atmospheric transport may persist through subsequent deposition and cycling.

Multiple Regression for ^{210}Pb Partitioning. In the general model for $f_P{}^{Pb}$ [R^2 = 38%], significant effects emerge from p_C [$e*$ = 37%] and season [9%], and none from pH (Figure 4c). Seasonality includes a spring maximum and winter minimum. Stepwise addition of specific MTE variables explains an additional 25% of variance with a total of five explanators [R^2 = 0.68]. In this second model, associations of f^{Pb} with MTEs are weak, and the strongest explanator was the concentration d.^{210}Pb [35%]. Here, N$_C$ or C$_C$ supersedes p_C [16%]. Other significant, positive correlations include d.S [8%], d.Fe [3%,] and d.Mn [3%]. There was a significant meteorological effect with continental convective storms favoring higher f^{Pb} [3%]. The modeled K_D for ^{210}Pb shows explanators and effects similar to those for f_P (s.S, d.Mn, d.^{210}Pb, event type), and these results are illustrated in Figure SI 5b.

In summary, ^{210}Pb partitioning is best predicted by its own concentration in an autocorrelative effect that we interpret, like p.c.e., as an indication of nonequilibrium behavior and control of ^{210}Pb partitioning by colloids. $f_P{}^{Pb}$ shows no significant, direct pH dependence. In TF deposition and soils, ^{210}Pb mobility is regulated by organic colloids,[48,62,63] though here we are not able to constrain this effect with, e.g., measurements of dissolved organic carbon. The role of organic matter in ^{210}Pb partitioning is also supported by correlations with N$_C$ favoring particulate and d.Fe favoring dissolved ^{210}Pb; Fe, too, is regulated by organic colloids.[48,60] We suggest that a positive correlation of f^{Pb} with d.S indicates formation of insoluble PbSO$_4$. While solubility products for PbSO$_4$ in both bulk precipitation and desorption experiments are 2 orders of magnitude lower than the governing equilibrium constant (K_{sp} PbSO$_4$ = 10^{-8}), PbSO$_4$ is a major Pb phase in natural aerosols.[64,65] We have also observed a strong, independent correlation between ^{210}Pb and SO$_4$ fluxes in bulk deposition over both event and interannual scales that is consistent with the influence of ^{210}PbSO$_4$ on aerosol scavenging.[36] An additional correlation of f^{Pb} with d.Mn is consistent with the known affinity of Pb for Mn oxides.[66,38] Finally, the influence of convective storms on ^{210}Pb partitioning suggests that the entrainment of terrestrial aerosols could include the resuspension of recycled PM. Similar to the case for ^{7}Be, the presence of convective storms and S in models of both speciation and deposition[36] for ^{210}Pb suggests that the atmospheric speciation of ^{210}Pb persists in postdepositional cycling.

Discriminating FRNs with Multiple Regression for the Ratio f^{Be}:f^{Pb}. We modeled the ratio f^{Be}:f^{Pb} to confirm that it was predicted by the same explanators that influence f^{Be} and f^{Pb} (Figure 4e,f). A model using environmental variables [R^2 = 60%] shows significant effects from p_C [$e*$ = 33%], pH [18%], season [10%], and storm type [5%]. Adding specific variables improves the model [R^2 = 76%] with five significant explanators including positive correlations with s.Mn [36%] and pH [14%] and inverse correlations with d.Al [10%] and s.Ni [3%]. Here, s.Mn, d.Al, and pH influence the ratio as expected from effects on f^{Be}. While Mn showed positive effects on both $f_P{}^{Be}$ and $f_P{}^{Pb}$, here it favors ^{7}Be. Neither N$_C$ nor C$_C$ appear in the model, suggesting that organic matter does not discriminate between the FRNs. Finally, seasonality showed a bias for higher ^{210}Pb partitioning in autumn [3%]. Autumn precipitation is distinguished by high Mn and anthropogenic metal concentrations[36] (Table SI 2), all of which are cycled strongly through tree canopies.[48,67,68] In conjunction with ^{210}Pb, these may indicate the resuspension of biogenic aerosols following the annual cycle of tree leaf senescence.

Resuspended Aerosols and a Particle-Age Effect (p.a.e.) in FRN Partitioning: Insights from ^{10}Be. Because the FRNs have different half-lives, aerosol and particle age are

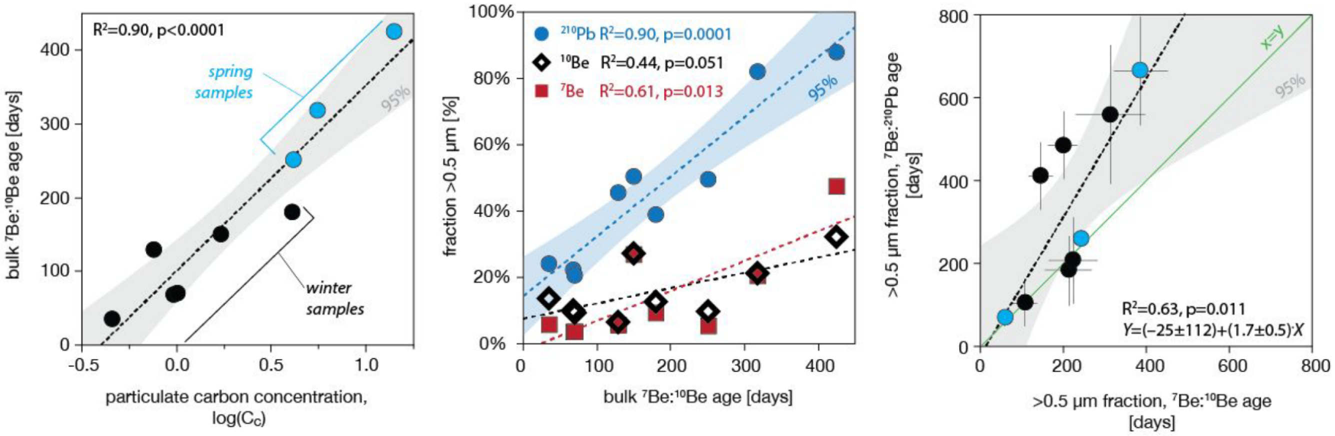

Figure 5. (a) ^{7}Be:^{10}Be age of bulk deposition versus particulate carbon concentration (C_C) for spring and winter, which are seasons of maximum and minimum C_C, respectively. (b) Dependence of fractions-particulate on bulk age for ^{7}Be, ^{10}Be, and ^{210}Pb, and (d) age concordance plot of ^{7}Be:^{10}Be and ^{7}Be:^{210}Pb for the >0.5 μm fraction.

likely to exert a definitive control on their FRN ratios.[36] Based on our observation that FRN sorption is irreversible, we anticipated that FRN partitioning would increase with age as FRN aerosols interact with terrestrial PM. Such a particle-age effect (p.a.e.) would enhance the abundance of longer-lived FRNs in resuspended and recycled deposition and may contribute, for example, to higher K_D for ^{210}Pb in convective storms and in bulk versus wet-only deposition (Figure 1).

To investigate age effects on FRN partitioning, we measured abundances of ^{10}Be (half-life = 1.39×10^{6} years) in a small subset of paired "A" and "B" samples ($n = 9$) from spring and winter that represented the highest and lowest PM concentrations (Table SI 3). ^{7,10}Be isotopes should not fractionate, and their ratio can be interpreted unambiguously as a function of mean aerosol age.[44] We calculate ^{7,10}Be ages for bulk deposition using an open-system model, since this approach has proven accurate in measuring exposure times of tree leaves to FRN deposition[14]

$$\left(\frac{^{7}\mathrm{Be}}{^{10}\mathrm{Be}}\right) = P\cdot\frac{\lambda^{10}}{\lambda^{7}}\cdot\frac{1 - e^{\lambda^{7}t}}{1 - e^{\lambda^{10}t}} \tag{8}$$

Here, (^{7}Be/^{10}Be) is the observed atom ratio, P is the production ratio here assumed a constant = 1.88,[69] λ is the respective decay constant, and mean age t is solved by least-squares minimization. ^{7,10}Be ages for bulk deposition averaged 176 ± 45 days (±SE, $n = 9$). This is about 3.5 times older than if using a decay-only model (66 ± 14 days, similar to Graham et al.[44]), but either case is much older than the 4−14 days accepted for boundary layer aerosols via short-lived ^{210}Bi:^{210}Pb or ^{210}Po:^{210}Pb FRN chronometers.[70−73] Older ^{7,10}Be ages reflect some contribution of stratospheric ^{7,10}Be aerosols, for which residence times are ~1 year,[18] and recycled, resuspended PM in bulk deposition. As evidence for a recycled fraction, calculated ^{7}Be:^{10}Be ages are strongly correlated with p_C [$R^2 = 0.69$, $p = 0.006$] and more so with C_C [$R^2 = 0.90$, $p < 0.0001$, Figure 5a].

Importantly, differing ^{7,10}Be ages confirm that filtered fractions of bulk deposition are geochemically distinct and not in equilibrium.[74] The >0.5 μm fraction of bulk deposition is significantly older than the filter-passing fraction, 260 ± 45 versus 120 ± 30 days, respectively [mean ± SE, $p = 0.011$]. This difference is consistent with both a particulate fraction that is irreversibly sorbed and an operationally dissolved fraction that is colloidal. Moreover, f^{Be}, f^{Pb}, and f^{Be10} each increase significantly with calculated bulk ages (Figure 5b).

While it is not obvious that a ^{7,10}Be age should be valid for ^{210}Pb, given different origins for the FRNs, age is a better predictor for f^{Pb} [$R^2 = 0.90$] than either p_C [$R^2 = 0.60$] or C_C [$R^2 = 0.69$]. This aged fraction has proven difficult to isolate, identify, or characterize[75,76,36] but is likely to be important to both MTE ecosystem mass balance[10] and pollutant fate[77,11]—direct measurements of aerosol ages will likely provide new insights into these problems.

That age dependencies of f^{Be} and f^{Be10} are weak relative to f^{Pb} underscores different processes or consequences for aging of ^{7,10}Be versus ^{210}Pb aerosols. Higher solubilities or slower sorption kinetics of ^{7,10}Be aerosols and colloids might contribute to this difference. It might also reflect where aerosol aging occurs—while the ^{7,10}Be isotopes have longer residence times in the atmosphere as a consequence of their production bias to the stratosphere, ^{210}Pb is produced in the lower atmosphere where it presumably has greater interaction with terrestrial PM. This source effect is evident, for example, in the control of both ^{7}Be and ^{210}Pb speciation by the same meteorological and chemical factors that also influence their rates of deposition. We emphasize that these source effects are profound and fractionate even stable Pb and ^{210}Pb isotopes during both deposition[78] and subsequent interaction with vegetation.[79]

To better describe fractionation between ^{7,10}Be and ^{210}Pb in PM, we plotted concordance between ^{7,10}Be and ^{7}Be:^{210}Pb chronometers (Figure 5c). We note that these ratios continue to be governed by ongoing accumulation of the longer-lived nuclide once ^{7}Be has reached steady state at ca. 1 year. This means that the chronometer remains valid for timeframes spanning months to decades or centuries,[14,15] provided that a constant-flux assumption is met. A ^{7}Be:^{210}Pb age estimate is not possible for bulk deposition, because there is no fixed production ratio that corresponds to time zero. Instead, we estimated ^{7}Be:^{210}Pb ages of >0.5 μm particulates by assuming an initial activity ratio equal to that of flux-weighted bulk deposition of the preceding 4 weeks. This yielded ^{7}Be:^{210}Pb ages of 359 ± 71 days (mean ± SE, $n = 9$). These were older than corresponding ^{7,10}Be ages by a factor of 1.4 [$p = 0.062$]. The statistical significance of their difference is equivocal, yet correlation between the two systems is nonetheless strong [R^2

= 0.63, p = 0.011, Figure 5c]. We view this as affirmation that p.a.e. is a general phenomenon that influences aerosols of different origins and through which terrestrial PM incorporates multiple aerosol populations through an aerosol–particle transition. In this manner, despite differences in the magnitudes and chemistries of factors that regulate each FRN's partitioning to natural PM, their irreversibility of sorption and coarsening of particulate size distributions through time represent a foundation for FRN chronometry.

Implications for Terrestrial Aerosol Cycling, FRN Chronometry, and Tracer Applications. That FRNs establish stable associations with particulate matter provides an opportunity to trace aerosols through complex biogeochemical pathways, at timeframes that are otherwise difficult to capture. Critically, commonalities shown here between FRNs and other aerosol species including Al, Fe, Mn, Ni, Cr, V, Hg, P, C, and N build confidence that FRNs can help to understand cycling of other elements from atmosphere to vegetation, to soil and sediment.[80] Many aerosol budgets are confounded by the inability to otherwise distinguish novel from recycled deposition and this likely contributes to vast discrepancies between measured and modeled rates of aerosol deposition.[10] FRNs, on the other hand, record processes over defined timeframes. With its short half-life, ^{7}Be records only aerosol deposition at the event scale and thus provides a means for tracing the behavior and interactions of novel accumulation-mode aerosol deposition. In a similar way, ^{210}Pb and ^{10}Be are sufficiently long-lived to provide an index for aerosol stable isotopes in long-range transport. Excess deposition of other aerosol species relative to ^{210}Pb or ^{10}Be can thus be attributed to local resuspension and recycled deposition or, as in the case of Hg, to gaseous dry processes.

By combining FRNs, ^{7}Be:^{210}Pb (or ^{7}Be:^{10}Be) ratios provide estimates of the characteristic recycling times of aerosols. We have already shown that a recycled fraction of aerosol deposition persists in (re)circulation for a mean lifetime of ca. 200 days. Origin and dynamics of this fraction are not understood, but large aerosol reservoirs sit in long-lived tissues of the forest canopy (lichen, moss, bark, etc., collectively "phyllosphere"),[77] for example, storing a ∼5 year equivalent of total Hg atmospheric deposition on an areal basis.[81] FRN chronometry provides a means for estimating residence times and fluxes, across such biogeochemical boundaries that otherwise remain challenging to quantify.[82]

For geomorphic tracer applications, the irreversibility of FRN sorption reinforces our confidence that FRNs maintain particle fidelity through erosion and redistribution. Moreover, our results support bulk soil/sediment as a sampling medium, since ^{7}Be and ^{210}Pb partitioning ratios converge to unity at very low particulate concentrations (p_C), less than 100 mg L^{-1}. Here, the ^{7}Be:^{210}Pb chronometer and Linked Radionuclide aCcumulation (LRC) age model provide chronometry, bridging atmospheric to soil and sedimentary processes for time scales ranging from months to decades to centuries.[14,15] While dating of aggregate soils/sediments is justified, we have also shown that FRN speciation is likely to evolve with time from aerosols in atmospheric (re)circulation to accumulation in terrestrial particulate matter. Thus, at the grain scale, FRN speciation may still record aerosol sources, chemistries, and depositional processes, as moderated by a particle-age effect. We anticipate that future studies of FRN speciation might provide insight into rates of early diagenetic/pedogenic processes that mobilize/immobilize atmospheric metals in soils and sediments.

■ ASSOCIATED CONTENT

Supporting Information

The Supporting Information is available free of charge at https://pubs.acs.org/doi/10.1021/acs.est.1c03194.

> Supporting Text: Methods, Supporting Text: Comparison of "A" and "B" collectors, and Supporting Text: Multivariate analysis of major/trace elements; Figure SI 1: analytical methods flowchart; Figure SI 2: heterogeneity in FRN deposition; Figure SI 3: statistical methods flowchart; Figure SI 4: aerosol composition; Figure SI 5: multiple regression correlation webs for K_D; Table SI 1: environmental variables and bulk deposition of ^{7}Be and ^{210}Pb; Table SI 2: MTE concentrations of dissolved and soluble fractions of bulk deposition; Table SI 3: partition coefficients (K_D) for ^{7}Be and ^{210}Pb; Table SI 4: fractions particulate (f_P) for ^{7}Be and ^{210}Pb (PDF)

■ AUTHOR INFORMATION

Corresponding Author

Joshua D. Landis − *Department of Earth Sciences, Dartmouth College, Hanover, New Hampshire 03755, United States;* orcid.org/0000-0002-3039-7841;
Email: joshua.d.landis@dartmouth.edu

Authors

Carl E. Renshaw − *Department of Earth Sciences, Dartmouth College, Hanover, New Hampshire 03755, United States*
James M. Kaste − *Geology Department, The College of William and Mary, Williamsburg, Virginia 23187, United States*

Complete contact information is available at:
https://pubs.acs.org/10.1021/acs.est.1c03194

Funding

Contributions by CER to the work were supported by NSF EAR-1545623.

Notes

The authors declare no competing financial interest.
Data that support this manuscript may be found at 10.17632/t48y58mzfx.1.

■ ACKNOWLEDGMENTS

Special thanks to Paul Zietz and the Environmental Studies Program at Dartmouth College for measurements of C/N. Great thanks to Prof. Meredith Kelly for guidance, support, and unfailing encouragement in the Dartmouth Cosmogenic Isotope Lab. Constructive and informed comments from two anonymous reviewers improved this manuscript.

■ ABBREVIATIONS

K_D	equilibrium distribution coefficient [L kg^{-1}]
f_P	percent FRN activity in the >0.5 μm particulate fraction [%]
p_C	particle mass concentration [mg L^{-1}]
C_C	particulate C concentration [mg L^{-1}]
N_C	particulate N concentration [mg L^{-1}]
$t.C^P$	total particulate C mass [mg]
$t.N^P$	total particulate N mass [mg]

d.Al, etc.	operationally dissolved (<0.5 μm) element concentration [mg L^{-1}]
s.Al, etc.	2% HCl-soluble element concentration [mg L^{-1}]
t.Al, etc.	total 2% HCl-soluble element fraction [mg]
k.Al, etc.	relative element solubility index, *d*./*s*. [dimensionless]

■ REFERENCES

(1) Intergovermental Panel on Climate Change. Clouds and Aerosols. In *Climate Change 2013: The Physical Science Basis. Contribution of Working Group I to the Fifth Assessment Report of the Intergovernmental Panel on Climate Change*; Stocker, T. F., Qin, D., Plattner, G.-K., Tignor, M., Allen, S. K., Boschung, J., Nauels, A., Xia, Y., Bex, V., Midgley, P. M., Eds.; Cambridge University Press: Cambridge, 2014; pp 571−658.

(2) Kristiansen, N. I.; Stohl, A.; Olivié, D. J. L.; Croft, B.; Søvde, O. A.; Klein, H.; Christoudias, T.; Kunkel, D.; Leadbetter, S. J.; Lee, Y. H.; Zhang, K.; Tsigaridis, K.; Bergman, T.; Evangeliou, N.; Wang, H.; Ma, P.-L.; Easter, R. C.; Rasch, P. J.; Liu, X.; Pitari, G.; Di Genova, G.; Zhao, S. Y.; Balkanski, Y.; Bauer, S. E.; Faluvegi, G. S.; Kokkola, H.; Martin, R. V.; Pierce, J. R.; Schulz, M.; Shindell, D.; Tost, H.; Zhang, H. Evaluation of observed and modelled aerosol lifetimes using radioactive tracers of opportunity and an ensemble of 19 global models. *Atmos. Chem. Phys.* **2016**, *16* (5), 3525−3561.

(3) Wang, Y.; Xia, W.; Liu, X.; Xie, S.; Lin, W.; Tang, Q.; Ma, H. Y.; Jiang, Y.; Wang, B.; Zhang, G. J. Disproportionate control on aerosol burden by light rain. *Nat. Geosci.* **2021**, *14* (2), 72−76.

(4) Luo, X.; Bing, H.; Luo, Z.; Wang, Y.; Jin, L. Impacts of atmospheric particulate matter pollution on environmental biogeochemistry of trace metals in soil-plant system: A review. *Environ. Pollut.* **2019**, *255*, 113138.

(5) Mahowald, N. M.; Hamilton, D. S.; Mackey, K. R. M.; Moore, J. K.; Baker, A. R.; Scanza, R. A.; Zhang, Y. Aerosol trace metal leaching and impacts on marine microorganisms. *Nat. Commun.* **2018**, *9* (1), 2614.

(6) WHO, World Health Organization. *Ambient air pollution: A global assessement of exposure and burden of disease*; World Health Organization: Geneva, 2016.

(7) Costa, D. L.; Dreher, K. L. Bioavailable Transition Metals in Particulate Matter Mediate Cardiopulmonary Injury in Healthy and Compromised Animal Models. *Environ. Health Perspect.* **1997**, *105*, 1053−1060.

(8) Chen, L. C.; Lippmann, M. Effects of metals within ambient air particulate matter (PM) on human health. *Inhalation Toxicol.* **2009**, *21*, 1−31.

(9) Charrier, J. G.; Anastasio, C. On dithiothreitol (DTT) as a measure of oxidative potential for ambient particles: Evidence for the importance of soluble transition metals. *Atmos. Chem. Phys.* **2012**, *12* (19), 9321−9333.

(10) Saylor, R. D.; Baker, B. D.; Lee, P.; Tong, D.; Pan, L.; Hicks, B. B. The particle dry deposition component of total deposition from air quality models: right, wrong or uncertain? *Tellus, Ser. B* **2019**, *71* (1), 1550324.

(11) Yang, H.; Appleby, P. G. Use of lead-210 as a novel tracer for lead (Pb) sources in plants. *Sci. Rep.* **2016**, *6*, 21707.

(12) Obrist, D.; Kirk, J. L.; Zhang, L.; Sunderland, E. M.; Jiskra, M.; Selin, N. E. A review of global environmental mercury processes in response to human and natural perturbations: Changes of emissions, climate, and land use. *Ambio* **2018**, *47* (2), 116−140.

(13) Wu, M.; Liu, X.; Zhang, L.; Wu, C.; Lu, Z.; Ma, P. L.; Wang, H.; Tilmes, S.; Mahowald, N.; Matsui, H.; Easter, R. C. Impacts of Aerosol Dry Deposition on Black Carbon Spatial Distributions and Radiative Effects in the Community Atmosphere Model CAM5. *J. Adv. Model. Earth Syst.* **2018**, *10* (5), 1150−1171.

(14) Landis, J. D.; Renshaw, C. E.; Kaste, J. M. Quantitative Retention of Atmospherically Deposited Elements by Native Vegetation Is Traced by the Fallout Radionuclides ^{7}Be and ^{210}Pb. *Environ. Sci. Technol.* **2014**, *48*, 12022−12030.

(15) Landis, J. D.; Renshaw, C. E.; Kaste, J. M. Beryllium-7 and lead-210 chronometry of modern soil processes: The Linked Radionuclide aCcumulation model, LRC. *Geochim. Cosmochim. Acta* **2016**, *180*, 109−125.

(16) Koch, D.; Mann, M. Spatial and temporal variability of ^{7}Be surface concentrations. *Tellus, Ser. B* **1996**, *48*, 387−396.

(17) Dibb, J. E.; Talbot, R. W.; Gregory, G. L. Beryllium-7 and lead-210 in the western hemisphere Arctic atmosphere: observations from three recent aircraft-based sampling pograms. *J. Geophys. Res.* **1992**, *97* (D15), 16709.

(18) Delaygue, G.; Bekki, S.; Bard, E. Modelling the stratospheric budget of beryllium isotopes. *Tellus, Ser. B* **2015**, *67* (1), 28582.

(19) Liu, H.; Considine, D. B.; Horowitz, L. W.; Crawford, J. H.; Rodriguez, J. M.; Strahan, S. E.; Damon, M. R.; Steenrod, S. D.; Xu, X.; Kouatchou, J.; Carouge, C.; Yantosca, R. M. Using beryllium-7 to assess cross-tropopause transport in global models. *Atmos. Chem. Phys.* **2016**, *16* (7), 4641−4659.

(20) Kaste, J. M.; Heimsath, A. M.; Bostick, B. C. Short-term soil mixing quantified with fallout radionuclides. *Geology* **2007**, *35* (3), 243−246.

(21) Kaste, J. M.; Bostick, B. C.; Heimsath, A. M.; Steinnes, E.; Friedland, A. J. Using atmospheric fallout to date organic horizon layers and quantify metal dynamics during decomposition. *Geochim. Cosmochim. Acta* **2011**, *75* (6), 1642−1661.

(22) Jagercikova, M.; Cornu, S.; Bourlès, D.; Evrard, O.; Hatté, C.; Balesdent, J. Quantification of vertical solid matter transfers in soils during pedogenesis by a multi-tracer approach. *J. Soils Sediments* **2017**, *17* (2), 408−422.

(23) Wallbrink, P.; Murray, A. Use of fallout radionuclides as indicators of erosion processes. *Hydrol. Processes* **1993**, *7* (3), 297−304.

(24) Blake, W. H.; Wallbrink, P. J.; Wilkinson, S. N.; Humphreys, G. S.; Doerr, S. H.; Shakesby, R. A.; Tomkins, K. M. Deriving hillslope sediment budgets in wildfire-affected forests using fallout radionuclide tracers. *Geomorphology* **2009**, *104* (3−4), 105−116.

(25) Black, E.; Renshaw, C. E.; Magilligan, F. J.; Kaste, J. M.; Dade, W. B.; Landis, J. D. Determining lateral migration rates of meandering rivers using fallout radionuclides. *Geomorphology* **2010**, *123* (3−4), 364−369.

(26) Evrard, O.; Némery, J.; Gratiot, N.; Duvert, C.; Ayrault, S.; Lefèvre, I.; Poulenard, J.; Prat, C.; Bonté, P.; Esteves, M. Sediment dynamics during the rainy season in tropical highland catchments of central Mexico using fallout radionuclides. *Geomorphology* **2010**, *124* (1−2), 42−54.

(27) Willenbring, J. K.; von Blanckenburg, F. Meteoric cosmogenic Beryllium-10 adsorbed to river sediment and soil: Applications for Earth-surface dynamics. *Earth-Sci. Rev.* **2010**, *98* (1−2), 105−122.

(28) Bacon, A. R.; Richter, D. de B.; Bierman, P. R.; Rood, D. H. Coupling meteoric ^{10}Be with pedogenic losses of ^{9}Be to improve soil residence time estimates on an ancient North American interfluve. *Geology* **2012**, *40* (9), 847−850.

(29) Wittmann, H.; von Blanckenburg, F.; Dannhaus, N.; Bouchez, J.; Gaillardet, J.; Guyot, J. L.; Maurice, L.; Roig, H.; Filizola, N.; Christl, M. A test of the cosmogenic ^{10} Be(meteoric)/ ^{9} Be proxy for simultaneously determining basin-wide erosion rates, denudation rates, and the degree of weathering in the Amazon basin. *J. Geophys. Res. Earth Surf.* **2015**, *120*, 2498−2528.

(30) Matisoff, G.; Wilson, C. G.; Whiting, P. J. The 7Be/210Pbxs ratio as an indicator of suspended sediment age or fraction new sediment in suspension. *Earth Surf. Processes Landforms* **2005**, *30* (9), 1191−1201.

(31) Yang, W.; Guo, L.; Chuang, C. Y.; Schumann, D.; Ayranov, M.; Santschi, P. H. Adsorption characteristics of ^{210}Pb, ^{210}Po and ^{7}Be onto micro-particle surfaces and the effects of macromolecular organic compounds. *Geochim. Cosmochim. Acta* **2013**, *107*, 47−64.

(32) Chuang, C. Y.; Santschi, P. H.; Ho, Y. F.; Conte, M. H.; Guo, L.; Schumann, D.; Ayranov, M.; Li, Y. H. Role of biopolymers as major carrier phases of Th, Pa, Pb, Po, and Be radionuclides in settling particles from the atlantic ocean. *Mar. Chem.* **2013**, *157*, 131−143.

(33) Chuang, C. Y.; Santschi, P. H.; Wen, L. S.; Guo, L.; Xu, C.; Zhang, S.; Jiang, Y.; Ho, Y. F.; Schwehr, K. A.; Quigg, A.; Hung, C.-C.; Ayranov, M.; Schumann, D. Binding of Th, Pa, Pb, Po and Be radionuclides to marine colloidal macromolecular organic matter. *Mar. Chem.* **2015**, *173*, 320−329.

(34) Boschi, V.; Willenbring, J. K. The effect of pH, organic ligand chemistry and mineralogy on the sorption of beryllium over time. *Environ. Chem.* **2016**, *13* (4), 711−722.

(35) Lin, P.; Xu, C.; Xing, W.; Sun, L.; Kaplan, D. I.; Fujitake, N.; Yeager, C. M.; Schwehr, K. A.; Santschi, P. H. Radionuclide uptake by colloidal and particulate humic acids obtained from 14 soils collected worldwide. *Sci. Rep.* **2018**, *8* (1), 4795.

(36) Landis, J. D.; Feng, X.; Kaste, J. M.; Renshaw, C. E. Aerosol populations, processes and ages contributing to bulk atmospheric deposition: insights from a 9-year study of ^{7}Be, ^{210}Pb, sulfate and major/trace elements. *J. Geophys. Res. Atmos.* **2021**, *in press*. Preprint available at: https://www.essoar.org/doi/10.1002/essoar.10507641.1.

(37) Takahashi, Y.; Minai, Y.; Ambe, S.; Makide, Y.; Ambe, F. Comparison of adsorption behavior of multiple inorganic ions on kaolinite and silica in the presence of humic acid using the multitracer technique. *Geochim. Cosmochim. Acta* **1999**, *63* (6), 815−836.

(38) Schroth, A. W.; Bostick, B. C.; Kaste, J. M.; Friedland, A. J. Lead sequestration and species redistribution during soil organic matter decomposition. *Environ. Sci. Technol.* **2008**, *42* (10), 3627−3633.

(39) Cuss, C. W.; Glover, C. N.; Javed, M. B.; Nagel, A.; Shotyk, W. Geochemical and biological controls on the ecological relevance of total, dissolved, and colloidal forms of trace elements in large boreal rivers: Review and case studies. *Environ. Rev.* **2020**, *28* (2), 138−163.

(40) Sedwick, P. N.; Sholkovitz, E. R.; Church, T. M. Impact of anthropogenic combustion emissions on the fractional solubility of aerosol iron: Evidence from the Sargasso Sea. *Geochem., Geophys., Geosyst.* **2007**, *8* (10), Q10Q06.

(41) Shelley, R. U.; Landing, W. M.; Ussher, S. J.; Planquette, H.; Sarthou, G. Regional trends in the fractional solubility of Fe and other metals from North Atlantic aerosols (GEOTRACES cruises GA01 and GA03) following a two-stage leach. *Biogeosciences* **2018**, *15* (8), 2271−2288.

(42) Creamean, J. M.; Lee, C.; Hill, T. C.; Ault, A. P.; DeMott, P. J.; White, A. B.; Ralph, F. M.; Prather, K. A. Chemical properties of insoluble precipitation residue particles. *J. Aerosol Sci.* **2014**, *76*, 13−27.

(43) Singleton, A. A.; Schmidt, A. H.; Bierman, P. R.; Rood, D. H.; Neilson, T. B.; Greene, E. S.; Bower, J. A.; Perdrial, N. Effects of grain size, mineralogy, and acid-extractable grain coatings on the distribution of the fallout radionuclides ^{7}Be, ^{10}Be, ^{137}Cs, and ^{210}Pb in river sediment. *Geochim. Cosmochim. Acta* **2017**, *197*, 71−86.

(44) Graham, I.; Ditchburn, R.; Barry, B. Atmospheric deposition of ^{7}Be and ^{10}Be in New Zealand rain (1996−98). *Geochim. Cosmochim. Acta* **2003**, *67* (3), 361−373.

(45) Baskaran, M. A search for the seasonal variability on the depositional fluxes of ^{7}Be and ^{210}Pb. *J. Geophys. Res.* **1995**, *100* (D2), 2833−2840.

(46) Landis, J. D.; Renshaw, C. E.; Kaste, J. M. Measurement of ^{7}Be in soils and sediments by gamma spectroscopy. *Chem. Geol.* **2012**, *291*, 175−185.

(47) Hou, H.; Takamatsu, T.; Koshikawa, M. K.; Hosomi, M. Trace metals in bulk precipitation and throughfall in a suburban area of Japan. *Atmos. Environ.* **2005**, *39* (20), 3583−3595.

(48) Gandois, L.; Tipping, E.; Dumat, C.; Probst, A. Canopy influence on trace metal atmospheric inputs on forest ecosystems: Speciation in throughfall. *Atmos. Environ.* **2010**, *44* (6), 824−833.

(49) Pan, G.; Liss, P. S. Metastable-Equilibrium Adsorption Theory. II. Experimental. *J. Colloid Interface Sci.* **1998**, *201* (1), 77−85.

(50) U.S. Environmental Protection Agency. *Understanding Variation in Partition Coefficient, K_d, values*; EPA 402-R-99-004A; U.S. Dept. Energy: Washington, D.C., 1999.

(51) O'Connor, D. J.; Connolly, J. P. The effect of concentration of adsorbing solids on the partition coefficient. *Water Res.* **1980**, *14* (10), 1517−1523.

(52) Honeyman, B. D.; Santschi, P. H. A Brownian-pumping model for oceanic trace metal scavenging: evidence from Th isotopes. *J. Mar. Res.* **1989**, *47* (4), 951−992.

(53) Benoit, G. Evidence of the particle concentration effect for lead and other metals in fresh waters based on ultraclean technique analyses. *Geochim. Cosmochim. Acta* **1995**, *59* (13), 2677−2687.

(54) Gründel, M.; Porstendörfer, J. Differences between the activity size distributions of the different natural radionuclide aerosols in outdoor air. *Atmos. Environ.* **2004**, *38* (22), 3723−3728.

(55) Degryse, F.; Smolders, E.; Parker, D. R. Partitioning of metals (Cd, Co, Cu, Ni, Pb, Zn) in soils: concepts, methodologies, prediction and applications - a review. *Eur. J. Soil Sci.* **2009**, *60* (4), 590−612.

(56) Gormley-Gallagher, A. M.; Douglas, R. W.; Rippey, B. The applicability of the distribution coefficient, KD, based on non-aggregated particulate samples from lakes with low suspended solids concentrations. *PLoS One* **2015**, *10* (7), No. e0133069.

(57) You, C.; Lee, T.; Li, Y. The partition of Be between soil and water☆. *Chem. Geol.* **1989**, *77* (2), 105−118.

(58) Brown, E.; Edmond, J.; Raisbeck, G.; Bourles, D.; Yiou, F.; Measures, C. Beryllium isotope geochemistry in tropical river basins. *Geochim. Cosmochim. Acta* **1992**, *56* (4), 1607−1624.

(59) Spokes, L. J.; Jickells, T. D.; Lim, B. Solubilisation of aerosol trace metals by cloud processing: A laboratory study. *Geochim. Cosmochim. Acta* **1994**, *58* (15), 3281−3287.

(60) Wang, Z.; Fu, H.; Zhang, L.; Song, W.; Chen, J. Ligand-Promoted Photoreductive Dissolution of Goethite by Atmospheric Low-Molecular Dicarboxylates. *J. Phys. Chem. A* **2017**, *121* (8), 1647−1656.

(61) Mao, J.; Fan, S.; Horowitz, L. W. Soluble Fe in Aerosols Sustained by Gaseous HO_2 Uptake. *Environ. Sci. Technol. Lett.* **2017**, *4* (3), 98−104.

(62) Miller, E. K.; Friedland, a J. Lead migration in forest soils: response to changing atmospheric inputs. *Environ. Sci. Technol.* **1994**, *28* (4), 662−669.

(63) Kaste, J. M.; Friedland, A. J.; Miller, E. K. Potentially mobile lead fractions in montane organic-rich soil horizons. *Water, Air, Soil Pollut.* **2005**, *167*, 139−154.

(64) Kersten, M.; Kriews, M.; Förstner, U. Partitioning of trace metals released from polluted marine aerosols in coastal seawater. *Mar. Chem.* **1991**, *36* (1−4), 165−182.

(65) Sakata, K.; Sakaguchi, A.; Yokoyama, Y.; Terada, Y.; Takahashi, Y. Lead speciation studies on coarse and fine aerosol particles by bulk and micro X-ray absorption fine structure spectroscopy. *Geochem. J.* **2017**, *51* (3), 215−225.

(66) Villalobos, M.; Bargar, J.; Sposito, G. Mechanisms of Pb(II) sorption on a biogenic manganese oxide. *Environ. Sci. Technol.* **2005**, *39* (2), 569−576.

(67) Rea, A. W.; Lindberg, S. E.; Keeler, G. J. Dry deposition and foliar leaching of mercury and selected trace elements in deciduous forest throughfall. *Atmos. Environ.* **2001**, *35* (20), 3453−3462.

(68) Rea, A. W.; Lindberg, S. E.; Scherbatskoy, T.; Keeler, G. J. Mercury accumulation in foliage over time in two northern mixed-hardwood forests. *Water, Air, Soil Pollut.* **2002**, *133* (1−4), 49−67.

(69) Heikkilä, U.; Beer, J.; Alfimov, V. Beryllium-10 and beryllium-7 in precipitation in Dübendorf (440 m) and at Jungfraujoch (3580 m), Switzerland (1998−2005). *J. Geophys. Res.* **2008**, *113* (D11), D11104.

(70) Moore, H. E.; Poet, S. E.; Martell, E. A. ^{222}Rn, ^{210}Pb, ^{210}Bi, and ^{210}Po profiles and aerosol residence times versus altitude. *J. Geophys. Res.* **1973**, *78* (30), 7065−7075.

(71) Gaffney, J. S.; Marley, N. A.; Cunningham, M. M. Natural radionuclides in fine aerosols in the Pittsburgh area. *Atmos. Environ.* **2004**, *38* (20), 3191−3200.

(72) Lozano, R. L.; San Miguel, E. G.; Bolívar, J. P.; Baskaran, M. Depositional fluxes and concentrations of ^{7}Be and 210Pb in bulk precipitation and aerosols at the interface of Atlantic and

Mediterranean coasts in Spain. *J. Geophys. Res.* **2011**, *116* (D18), D18213.

(73) Długosz-Lisiecka, M.; Bem, H. Determination of the mean aerosol residence times in the atmosphere and additional 210Po input on the base of simultaneous determination of ^{7}Be, ^{22}Na, ^{210}Pb, ^{210}Bi and ^{210}Po in urban air. *J. Radioanal. Nucl. Chem.* **2012**, *293* (1), 135−140.

(74) Francis, C. W.; Chesters, G.; Haskin, L. A. Determination of ^{210}Pb Mean Residence Time in the Atmosphere. *Environ. Sci. Technol.* **1970**, *4* (7), 586−589.

(75) Tokieda, T.; Yamanaka, K.; Harada, K.; Tsunogai, S. Seasonal variations of residence time and upper atmospheric contribution of aerosols studied with Pb-210, Bi-210, Po-210 and Be-7. *Tellus, Ser. B* **1996**, *48* (5), 690−702.

(76) Graly, J. A.; Reusser, L. J.; Bierman, P. R. Short and long-term delivery rates of meteoric ^{10}Be to terrestrial soils. *Earth Planet. Sci. Lett.* **2011**, *302* (3−4), 329−336.

(77) Farmer, J. G.; Eades, L. J.; Graham, M. C.; Cloy, J. M.; Bacon, J. R. A comparison of the isotopic composition of lead in rainwater, surface vegetation and tree bark at the long-term monitoring site, Glensaugh, Scotland, in 2007. *Sci. Total Environ.* **2010**, *408* (17), 3704−3710.

(78) Talbot, R. W.; Andren, A. W. Relationships between Pb and ^{210}Pb in aerosol and precipitation at a semiremote site in northern Wisconsin. *J. Geophys. Res.* **1983**, *88* (C11), 6752−6760.

(79) Shotyk, W.; Kempter, H.; Krachler, M.; Zaccone, C. Stable (^{206}Pb, ^{207}Pb, ^{208}Pb) and radioactive (^{210}Pb) lead isotopes in 1year of growth of Sphagnum moss from four ombrotrophic bogs in southern Germany: Geochemical significance and environmental implications. *Geochim. Cosmochim. Acta* **2015**, *163*, 101−125.

(80) Renshaw, C. E.; Dethier, E. N.; Landis, J. D.; Kaste, J. M. Seasonal and longitudinal variations in suspended sediment connectivity between river channels and their riparian margins. *ESS Open Archive* **2021** https://www.essoar.org/doi/10.1002/essoar.10508019.1.

(81) Wang, X.; Yuan, W.; Lin, C.-J.; Luo, J.; Wang, F.; Feng, X.; Fu, X.; Liu, C. Underestimated sink of atmospheric mercury in a deglaciated forest chronosequence. *Environ. Sci. Technol.* **2020**, *54*, 8083−8093.

(82) Sohrt, J.; Lang, F.; Weiler, M. Quantifying components of the phosphorous cycle in temperate forests. *Wiley Interdiscip. Rev.: Water* **2017**, *4*, e1243.

■ NOTE ADDED AFTER ASAP PUBLICATION

This paper was published ASAP on October 8, 2021, with an incorrect version of Figure 3. The corrected version was reposted on October 11, 2021.